Investigation of the La_2O_3-Nb_2O_5-WO_3 ternary phase diagram: Isolation and crystal structure determination of the original La_3NbWO_{10} material

T.D. Vu, T.D. Vu, M. Barre, K. Adil, A. Jouanneaux, E. Suard, F. Goutenoire

www.elsevier.com/locate/yjssc

PII: S0022-4596(15)00212-1
DOI: http://dx.doi.org/10.1016/j.jssc.2015.05.022
Reference: YJSSC18921

To appear in: *Journal of Solid State Chemistry*

Received date: 23 February 2015
Revised date: 15 May 2015
Accepted date: 17 May 2015

Cite this article as: T.D. Vu, T.D. Vu, M. Barre, K. Adil, A. Jouanneaux, E. Suard and F. Goutenoire, Investigation of the La_2O_3-Nb_2O_5-WO_3 ternary phase diagram: Isolation and crystal structure determination of the original La_3NbWO_{10} material, *Journal of Solid State Chemistry,* http://dx.doi.org/10.1016/j.jssc.2015.05.022

Journal of Solid State Chemistry 00 (2015) 1–11

Journal of Solid State Chemistry

Investigation of the La_2O_3-Nb_2O_5-WO_3 ternary phase diagram: Isolation and crystal structure determination of the original La_3NbWO_{10} material

T. D. Vu[b,], T. D. Vu[1,], M. Barre[1], K. Adil[b], A. Jouanneaux[1], E. Suard[c], F. Goutenoire[1]

[a] *IMMM (Institute of Materials and Molecules of Mans), UMR-CNRS 6283, University of Maine, 72085 Le Mans Cedex 9, France.*
[b] *KAUST (King Abdullah University of Science and Technology), Thuwal, Saudi Arabia.*
[c] *ILL ((Institute Lauë-Langevin), 6 J. Horowitz street, B P 156, 38042 Grenoble Cedex 9, France.*

Abstract

In the course of the exploration of the La_2O_3-WO_3-Nb_2O_5 ternary phase diagram, a new compound with the formula La_3NbWO_{10} was discovered. Its structure was determined from a combination of powder X-ray and neutron diffraction data. It crystallizes in the tetragonal space group $P4_2/nmc$ (n°137) with the lattice parameters: a = 10.0807(1) Å; c = 12.5540(1) Å. The structure is built up from infinite ribbons of octahedra $(W/Nb)O_5$ which are perpendicular to each other, lanthanum ions being distributed around these ribbons. The electrical properties of this compound were investigated on sintered pellets by means of complex impedance spectroscopy.

Keywords: Oxide, X-ray and neutron diffraction, Impedance spectroscopy.

1. Introduction

Since the 2000s, the development of hydrogen energy devices has raised the interest in discovering new materials with high oxygen conduction properties for the implementation in specific electrochemical systems such as SOFC (Solid Oxide Fuel Cell) [1, 2, 3]. Because of the low ionic conductivity of the currently used materials at low temperature, these devices operate at high temperatures leading to rapid aging and then degradation of their efficiency. Recently, the search for new compounds presenting high oxygen conductivities at lower temperatures led to the discovery of new molybdates and tungstates ($La_2Mo_2O_9$ [4], $Ba_{11}W_4O_{23}$ [5], $Sr_{11}Mo_4O_{23}$ [6], La_6WO_{12} [7] and $La_{10}W_2O_{21}$ [8]). Among them, $La_2Mo_2O_9$, which was evidenced from a global investigation of the La_2O_3-MoO_3 phase diagram, seems to be the most promising. This compound exhibits a polymorphism and crystallizes at low temperature in a very large supercell $(\times 2, \times 3, \times 4)$ where the oxygen atoms are ordered, while the high temperature form is a small cell $(\times 1, \times 1, \times 1)$ presenting an anionic disorder. This disorder allows the conduction by oxygen atoms [9]. The study of the La2O3-MoO3 phase diagram also led to the structural resolutions of $La_2Mo_4O_{15}$ [10] and $La_6Mo_8O_{33}$ [11] compounds which do not exhibit any conduction property. However, these previous investigations allowed to evidence a strong link between the compounds structures and their conduction properties. Such results show the great interest of phase diagram studies in order to discover new materials. In

☆Corresponding author, Tel: +33 652727130
Email address: tuong_dan.vu.etu@univ-lemans.fr (T. D. Vu)
URL: home page (T. D. Vu)

this purpose, we chose to explore the ternary diagram of La_2O_3-WO_3-Nb_2O_5.

In the past, different binary phase diagrams, La_2O_3-WO_3, WO_3-Nb_2O_5, have been studied by various groups, Yoshimura [12], Roth and Waring [13]. Most of the time, no structural information was obtained because of the lack of single crystals of good quality. To complete these works, we launched structural investigations in the La_2O_3-WO_3 system yielding the structure resolutions of α-$La_6W_2O_{15}$ [14], α-La_2WO_6 [15], β-La_2WO_6 [16], $La_{18}W_{10}O_{57}$ [17] and α-$La_2W_2O_9$ [18]. Now our work is focused on the ternary phase diagram La_2O_3-WO_3-Nb_2O_5 in which only one ternary material, $La_7Nb_3W_4O_{30}$, was discovered and mentioned in literature [19] until now.

In this paper, we present the synthesis of another phase in the diagram, La_3NbWO_{10}, together with its ab-initio structure determination from powder diffraction data and first results of electrical measurement.

2. Experimental

2.1. Material synthesis

The compound was prepared with La_2O_3, Nb_2O_5 and WO_3 as starting oxides. Lanthanum oxide powder was dried and decarbonated at 1000°C overnight prior to use. The oxides were weighed in stoichiometric proportions and ground together in an agate mortar. The prepared mixture was annealed in alumina crucible, according to the 4 successive steps presented in Table1, with intermediate grindings (heating and cooling rates: 10°C/min). The final powder is creamy white.

Table 1: Temperatures and durations of annealing procedure.

1^{st} time	at 1000°C in 2 h then at 1300°C in 10 h
2^{nd} time	at 1100°C in 2 h then at 1400°C in 52 h
3^{rd} time	at 1400°C in 65 h
4^{th} time	at 1400°C in 65 h

2.2. Material characterization

The room temperature X-ray diffraction (XRD) pattern was collected on a Bragg-Brentano diffractometer (MPD-PRO Panalytical) equipped with a linear detector X'Cellerator in the angular range from 5° to 150°(2θ), with a step size of 0.017° at λ = 1.5405 Å (copper target) for 10 hours. The thermal X-ray diffraction patterns were also acquired from 40 to 1000°C on the diffractometer with an Anton Paar HTK12 furnace.

The neutron diffraction (ND) pattern was obtained at room temperature using the D2B high-resolution/high-flux powder diffractometer at the Institute Lauë - Langevin in Grenoble, France. The data were acquired at 2θ intervals of 0.05° from 5° to 160° during 2 hours at λ = 1.5960 Å. The sample was packed in a vanadium can.

2.3. Electrochemical measurement

The transport property was studied by impedance spectroscopy using a Schlumberger Solartron SI 1260 frequency response analyzer with 0.1 V amplitude signal over the 32 MHz - 0.1 Hz frequency range. Five millimeter diameter pellets with, as electrodes, a thin platinum layer deposited on both faces were used for the measurements. The measurements were performed in air in the temperature range of 600-1000K (P_{O2} = 0.2 atm).

3. Results and discussion

3.1. Indexation and crystal symmetry determination

At the beginning, from the Search-Match procedure on X'Pert High Score Plus software [20], the non-stoichiometric phase $La_4W_3O_{15}$ [21] was identified as a similar structure to the title material (pdf 00-049-0972: tetragonal parameters a = 10.06 Å; c = 12.63 Å; Z = 4; space group $P4_2/nmc$). The relation between this phase and the title phase can be showed as:

$$La_4W_3O_{15} \times \frac{2}{3} \rightarrow La_{2.67}\square_{0.33}W_2O_{10} \leftrightarrow La_3NbWO_{10}$$

However, its crystallographic structure does not exist in the ICSD structural database. As mentioned in the paper [21], this isostructural compound was obtained in the ternary system La_2O_3-WO_3-NaCl. The initial ratio of the $La_2O_3$and WO_3 mixture was 1 : 3. The $La_4W_3O_{15}$ crystals grew under the vaporization of NaCl and, partially, WO_3. In order to re-synthesize $La_4W_3O_{15}$ compound, a solid-state synthesis was launched but without success. The obtained product was $La_{18}W_{10}O_{57}$ and $La_2W_2O_9$, its two adjacent phases on the phase diagram of La_2O_3-WO_3 system.

The indexation of the powder X-ray diffraction of La_3NbWO_{10} was carried out using the auto-indexing software Treor [22] implemented in FullProf program [23]. A satisfactory solution was obtained in tetragonal symmetry with a = 10.08 Å and c = 12.5 Å, V = 1270.08 Å^3 with a figure of merit M_{20} = 47 and F_{20} = 65 [24]. These cell constants are in a good agreement with the values determined from McMaille software [25] (M_{20} = 145.77 and F_{20} = 216.40).

The number of chemical formula units per unit cell (Z) was extrapolated using the average volume of oxygen (18-22 Å^3) in oxides combined with the nominal

composition of the compound La_3NbWO_{10} :

$$Z_{max} = \frac{1265.85}{18 \times 10} = 7.03$$

$$Z_{min} = \frac{1265.85}{22 \times 10} = 5.75$$

From the two possible extrema, it seems clear that the value Z = 6 is the best solution to respect the material composition.

To determine the space group of this compound, a Le Bail refinement procedure [23] was applied in space group P4/mmm (N°123) using the Fullprof program in order to extract the observed intensities of the individual reflections from the XRD pattern. In the range of low angles(below 27°(2θ)) (Figure 1), the peaks with indexation (111), (210), (003), (113) and (300) are absent, leading to the extinction conditions : hhl $l = 2n$, $hk0$ $h + k = 2n$, $00l$ $l = 2n$ and $h00$ $h = 2n$. These conditions leaded to space group $P4_2/nmc$ (N°137). Figure 1 shows a non-indexed peak of very low intensity at 25.6° (2θ) corresponding to the most intense peak of an unidentified impurity.

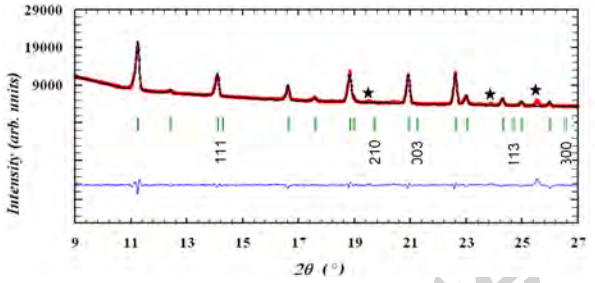

Figure 1: Le Bail refinement using space group P4/mmm : observed (points), calculated (line), difference profiles and reflection positions (ticks), impurity peaks (★).

3.2. Crystal structure determination

The first step of the structure determination consisted to localize the positions of heavy atoms (cations). The Monte Carlo analysis in the Espoir program [26] was launched in scratch mode using only the first 230 peaks (extracted by Le Bail refinement from the XRD data in space group $P4_2/nmc$).

For the determination of cationic positions, in order to minimize the number of different atom types, we replaced the mixed site (Nb/W) by a single atom Te (52e-) which represents an average of W^{6+} (68 e-) and Nb^{5+} (36 e-). Distance constraints (La-Te < 3.3 Å, La-La < 3.7 Å and Te-Te < 3.3 Å) were applied to the search of cationic positions. A first structural model was tested. It based on the distribution of 18 La atoms and 12 Te atoms over 4 crystallographic sites of multiplicities 16, 2, 8 and 4, leading to a R_{Bragg} value of 27.4%. In the second structural model, La and Te atoms were distributed over 5 crystallographic positions of multiplicities 8, 8, 2, 8 and 4, yielding a better R_{Bragg} value (18.7%). The first Rietveld refinement [27] on XRD data confirmed these five cationic positions, according to satisfactory R-factors (R_{Bragg} = 13.1%, R_{wp} = 23.0% and R_{exp} = 3.9%).

Fourier difference syntheses enabled four oxygen atoms to be easily determined while the two last oxygen positions remained quite difficult to locate. Nevertheless, after a fine analysis of the Fourier difference maps, these two oxygen sites were determined, leading to the final result of 60 oxygen atoms over 6 atomic positions. These positions were confirmed from the Rietveld refinement of the ND pattern as shown below.

As a last step, these structural information were then refined by launching a combined Rietveld refinement using XRD and ND data. The relative weightings of the XRD and ND data were 50:50. Nb and W atoms were statistically distributed over both crystallographic sites 8g and 4d. Their occupancies were refined and constrained to respect a total number of 6 W and 6 Nb atoms per unit cell.

The final combined Rietveld refinement of the appropriate atomic coordinates, occupancies, temperature factors along with the lattice constants, scale factors, zero-points, peak-shape parameters of the Thompson-Cox-Hastings [28] Pseudo-Voigt functions and background parameters converged to the R-factor values gathered in Table 2. Structural parameters are reported in Table 4. During the process, quite high B_{iso} values for La2 atoms (1.62 $Å^2$) were obtained, leading to unusual distributions on Fourier maps. Therefore, anisotropic temperature factors were refined for this position. That helped to lower significantly the R_{Bragg} (from 7.9 to 7.1 % on XRD data and from 8.5 to 7.6 % on ND data). This decision is justified by high values of both X-ray scattering factors and neutron scattering length. The observed, calculated and difference profiles are illustrated in Figures 2 and 3.

Table 2: Combined Rietveld refinement results.

Diffractometer	MPD-PRO	D2B(ILL)
Radiation	Cu-Kα	1.59600(5)
2θ range(°)	8 - 150	5 - 160
R_{Bragg} (%)	7.1	7.6
R_p (%)	12.5	12.3
R_{wp} (%)	13.3	13.3
R_{exp} (%)	3.7	3.6
Number of reflections	737	710
Total number of refined parameters: 69 (structural parameters: 34)		

Using the BondStr tool implemented in the Fullprof Suite, the valences of all atoms were also calculated showing a rather good agreement with the expected values: +3 for La, +(greater than 5 and less than 6) for (Nb/W) and -2 for O (Table 3).

Table 3: Bond-valences of atoms.

La1	3.14(2)	O1	2.19(1)
La2	2.58(2)	O2	1.92(2)
La3	3.63(1)	O3	1.87(1)
(Nb/W)1	5.46(6)	O4	1.88(2)
(Nb/W)2	5.28(5)	O5	1.92(5)
		O6	1.95(1)

Table 4: Crystallographic positions refined from mixed X-ray and neutron diffraction data of La_3NbWO_{10} : a = b = 10.0807(1) Å; c = 12.5540(1) Å; $P4_2/nmc$ (n°137); Z = 6.

Atom	Multiplicity	x	y	z	B_{iso} (Å^2)	Occupation
La1	8f	0.0216(1)	0.9784(1)	0.75	0.69(1)	1
La2	8g	0.75	0.9757(2)	0.5158(2)	1.62(*)	1
La3	2a	0.25	0.75	0.25	0.28(7)	1
W1	8g	0.75	0.0538(2)	0.9796(1)	0.30(4)	0.6775(1)
Nb1	8g	0.75	0.0538(2)	0.9796(1)	0.30(4)	0.3225(1)
W2	4d	0.75	0.75	0.2937(3)	0.41(7)	0.145(1)
Nb2	4d	0.75	0.75	0.2937(3)	0.41(7)	0.855(1)
O1	16h	0.3943(4)	0.6195(4)	0.3689(3)	0.61(6)	1
O2	16h	0.5388(5)	0.3910(5)	0.4242(4)	2.28(9)	1
O3	4c	0.75	0.25	0.4867(8)	2.5(2)	1
O4	8g	0.25	0.1294(6)	0.0610(5)	1.6(1)	1
O5	8g	0.25	0.3931(6)	0.2958(5)	1.2(1)	1
O6	8g	0.75	0.5566(5)	0.3155(5)	1.1(1)	1

	β_{11}	β_{22}	β_{33}	β_{12}	β_{13}	β_{23}
La2	0.0083(3)	0.0014(2)	0.0015(2)	0	0	-0.0009(2)

(*) equivalent displacement parameter (Å^2)

3.3. Structure Analysis

The structure of La_3NbWO_{10} is a superstructure of the Fluorite family (AX_2, a_F = 5.4 Å, Z = 4). It can be described as a supercell $(2a_F, 2a_F, 2a_F)$ with a lengthened cell parameter a_F along the c axis (6.2 Å). Hence the volume of La_3NbWO_{10} has to be 8 times bigger than that of the Fluorite cell. The Fluorite formula can now be written as $A_{32}X_{64}$ basing on the expression $4 \times 8 \times AX_2$. The formula La_3NbWO_{10} is consequently expressed as $La_{18}Nb_6W_6\square_2O_{60}\square_4$ with 2 cationic and 4 anionic vacancies.

$$\begin{pmatrix} a \\ b \\ c \end{pmatrix} = \begin{pmatrix} 2 & 0 & 0 \\ 0 & 2 & 0 \\ 0 & 0 & 2 \end{pmatrix} \times \begin{pmatrix} a_F \\ b_F \\ c_F \end{pmatrix}$$

$$V = 8 \times V_F$$

$$AX_2 \times 4 \times 8 \rightarrow A_{32}X_{64}$$

$$La_3NbWO_{10} \rightarrow La_{18}Nb_6W_6\square_2O_{60}\square_4$$

The structure is composed of 3 types of block: blocks of O1, blocks of O2, O3, and blocks of O4, O5,

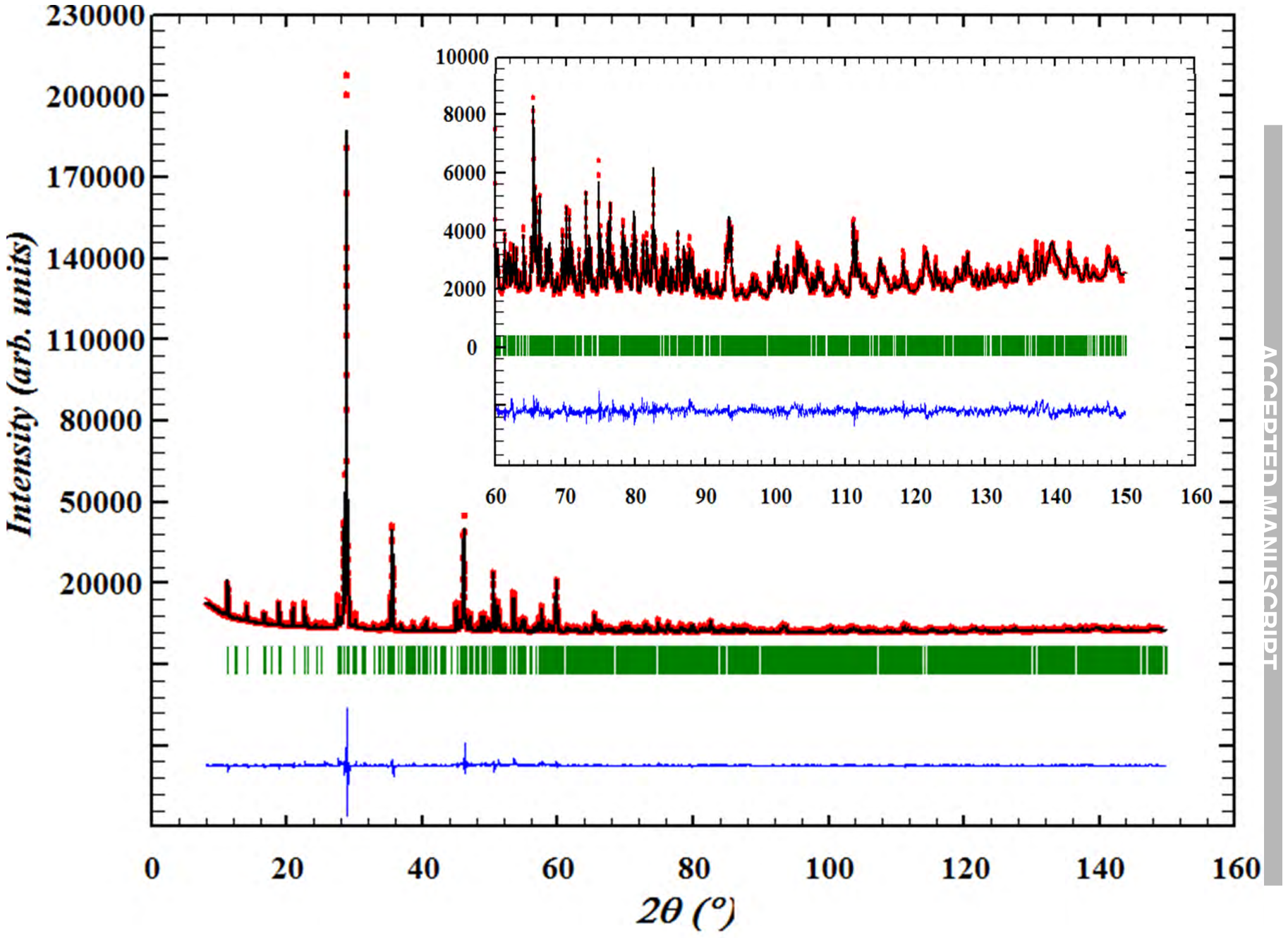

Figure 2: Fitted XRD diagram of La_3NbWO_{10} : observed (circles) and calculated (lines) data; reflections (vertical lines); and differences between observed and calculated data (bottom). The zoom-in section is in the inset.

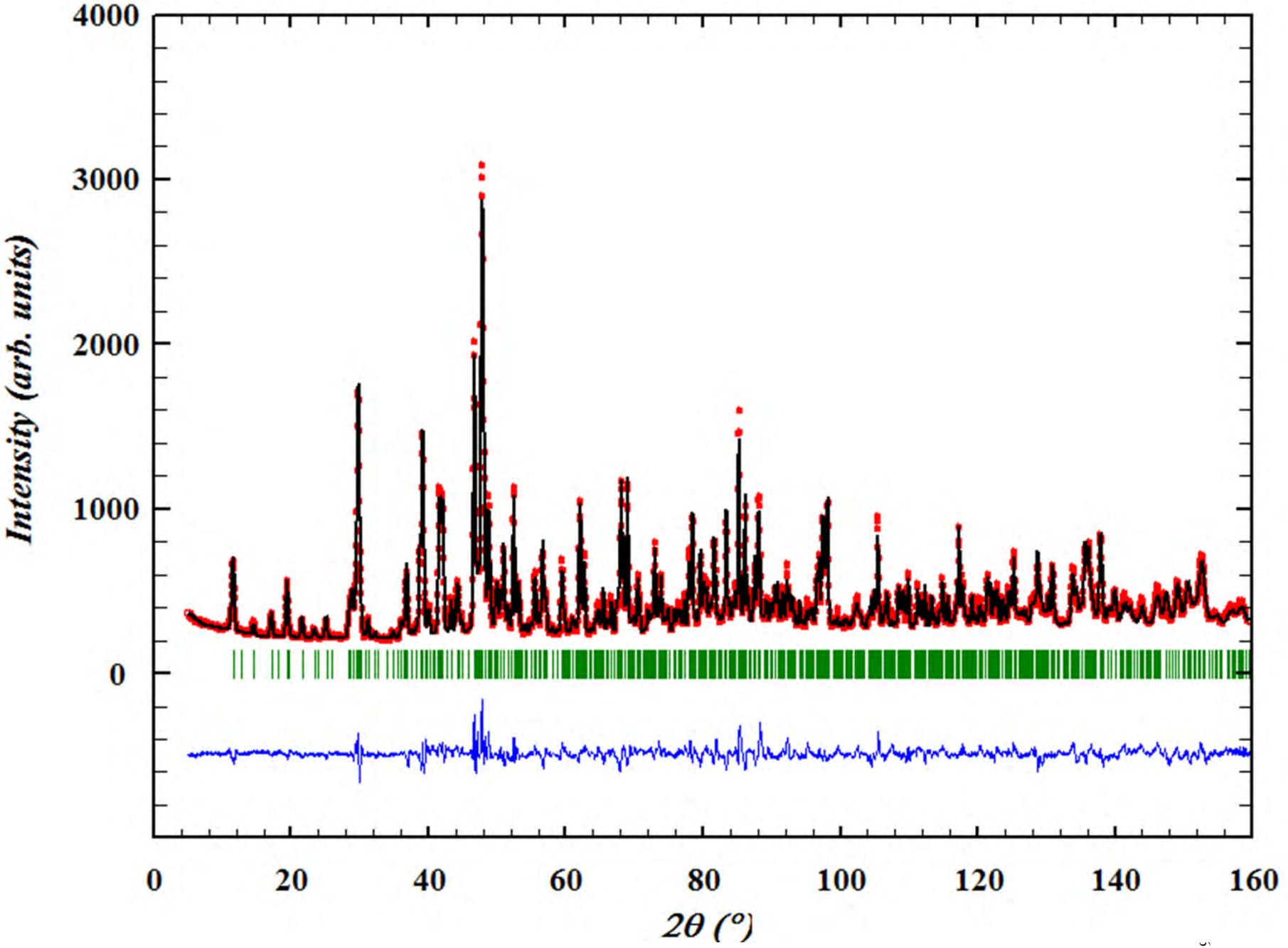

Figure 3: Fitted neutron diffraction diagram of La_3NbWO_{10} : observed (circles) and calculated (lines) data; reflections (vertical lines); and differences between observed and calculated data (bottom).

O6. In the first type, the O1 atoms are located in tetrahedral sites (Figure 4a). The arrangement of cations and anions is like in a Fluorite structure. In the second type, a cationic vacancy has been found in the middle of the block (Figure 4b). The coordination number of O2 and O3 atoms are 3 and 4, respectively. In the third type, the O4 and O6 atoms are in tetrahedral sites but the coordination number of O5 atoms is only 2 (Figure 4c).

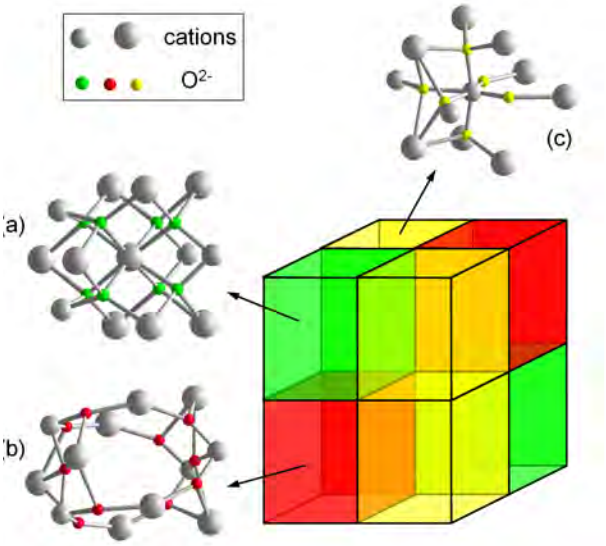

Figure 4: An unit cell of La_3NbWO_{10} composed of blocks.

A projection of cations of an unit cell along the c axis enables the cationic defaults to be observed (Figure 5). For a two-metal compound, the Fluorite formula is transformed into ABX_4, such as Scheelite tungstates $CaWO_4$ and $SrWO_4$ [29], which is illustrated in dashed cell. At z = 0.5c and z = c, the cations are nearly distributed over the expected positions of the Fluorite cell. A very small distortion is observed (Figure 5a). Meanwhile, at z = 0.25c and z = 0.75c, a cationic vacancy appears and a expected position of (Nb/W) is simultaneously occupied by a La atom. The two cationic vacancies are located on the 2b sites ((3/4,1/4,1/4) and (3/4,1/4,3/4)) (Figure 5b).

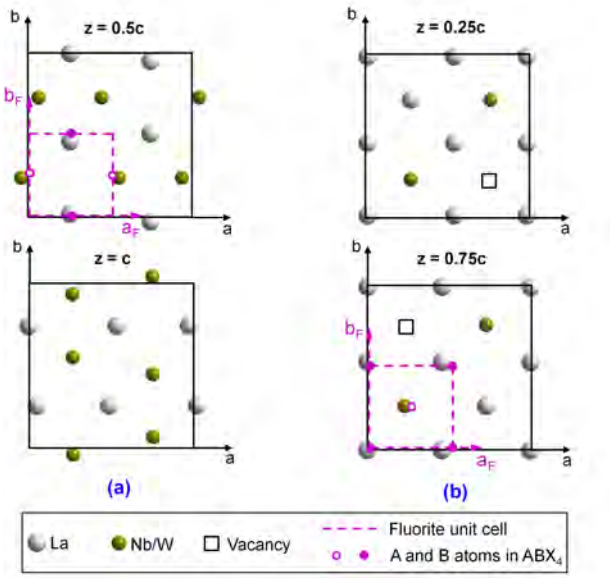

Figure 5: Projection along the c axis of only cationic positions of an La_3NbWO_{10} unit cell.

The anionic defaults can be also observed by looking at the coordinations around cations. All (Nb/W) atoms of the structure are surrounded by 6 oxygen atoms thus form octahedra. In contrast, La atoms present different coordinations, as shown in figure 6. At z = 0.5c (and z = c), there are 8 or 9 oxygen atoms around a La atom (Figure 6a). At z = 0.25c (and z = 0.75c), the coordination number of La atoms is 6 when they are near a cationic vacancy and 8 when they are on the mixed site.

The presence of these vacancies explains the high values of isotropic thermal factors for O2 and O3 atoms (2.3 and 2.5 $Å^2$ respectively) which are around the vacancies and can easily agitate in their large environments, consequently.

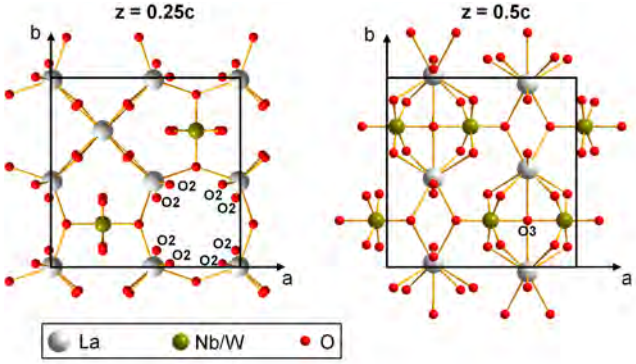

Figure 6: Projection along the c axis of cationic and anionic positions of an La_3NbWO_{10} unit cell.

In order to have a global view of the structure, the compound formula can be separated into two parts:

$$La_3(Nb/W)_2O_{10} \rightarrow [La_3] + 2 \times [(Nb/W)O_5]$$

According to this expression, the structure can be described by an infinity of layers composed of ribbons of $(Nb/W)O_5$ octahedra. Those quasi-regular octahedra are constructed with a central atom (Nb/W) and its six ligands (Figure 7a) with distances ranging from 1.830(0) Å to 2.193(6) Å and angles O-(Nb/W)-O close to 90° (Table 5). Each octahedron shares two corners with its neighbors (Figure 7b). All layers are perpendicular to the c axis (Figure 7c). Ribbons of the same layer are parallel, while ribbons of two adjacent layers are perpendicular to each other (Figure 7d, e). Lanthanum cations are distributed around these ribbons.

Table 5: Distances and angles in octahedra.

Distances (Å)			Angles (°)				
Nb1/W1	O2	2 × 1.872(5)	Nb1/W1	O1	O2	O3	O4
	O4	1.916(6)	O1	83.1(2)	2 × 88.2(2)	2 × 83.6(1)	2 × 93.9(1)
	O1	2 × 1.872(5)	O2		98.9(2)	2 × 86.8(2)	2 × 95.4(2)
	O3	2.023(3)					
Nb2/W2	O5	2 × 1.828(5)	Nb2/W2	O4	O5	O6	
	O6	2 × 1.969(5)	O4	67.4(1)	2 × 94.3(1)	4 × 83.4(1)	
	O4	2 × 2.191(6)	O5		104.1(1)	4 × 94.9(1)	

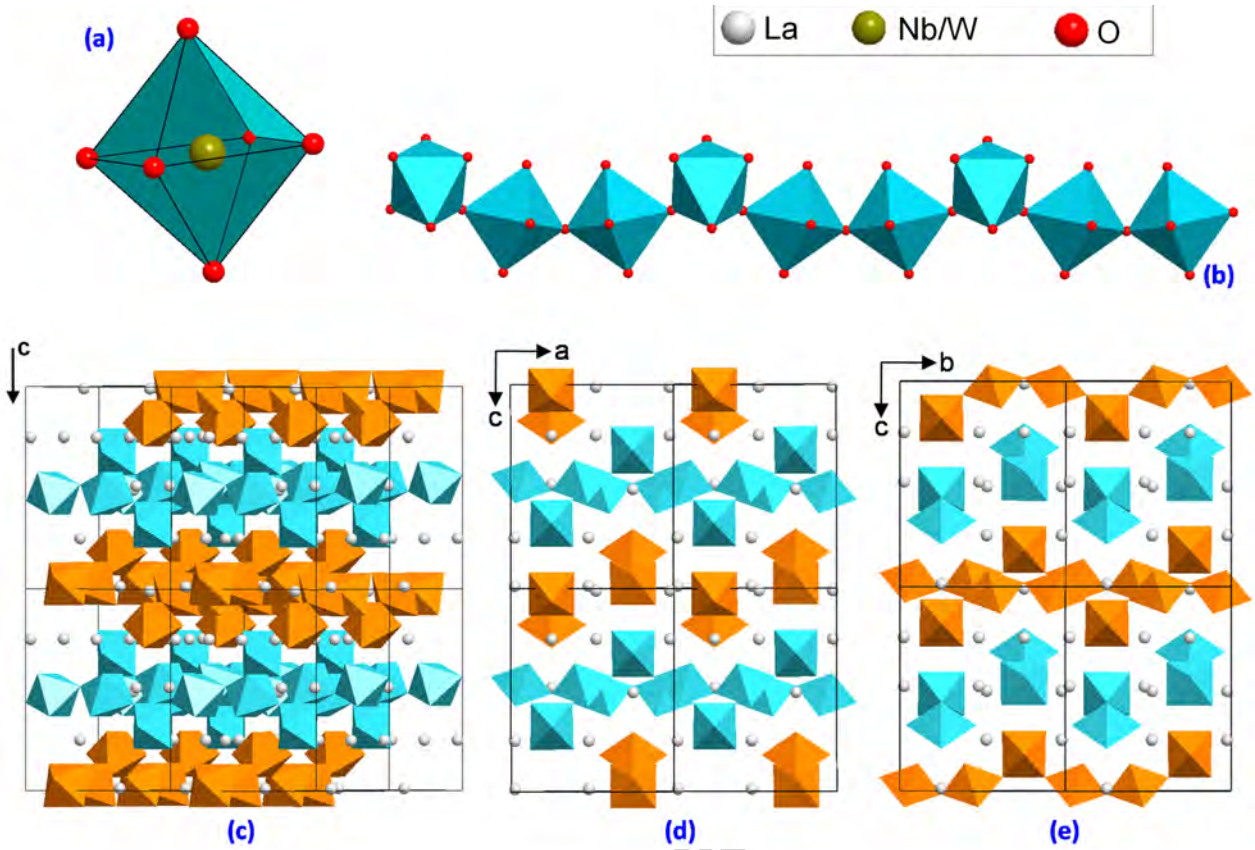

Figure 7: Illustration of the La_3NbWO_{10} structure: **(a)** an octahedron $(Nb/W)O_6$; **(b)** a ribbon of octahedra of formula $(Nb/W)O_5$; **(c)** layers perpendicular to the c axis; **(d)** view along the b axis; **(e)** view along the a axis (obtained by a 90°rotation of **(d)** around the c axis).

3.4. Impedance spectroscopy measurements and thermal expansion

High oxygen conduction was expected in La_3NbWO_{10} due to the presence of structural vacancies. Therefore, complex impedance spectroscopy measurements were carried out on sintered pellets. The ionic conductivity values for La_3NbWO_{10} are much lower than for the reference material Yttria Stabilized Zirconia (YSZ 8%) and $La_2Mo_2O_9$ which show ionic conductivity of around 0.05 $S.cm^{-1}$ at 800°C (Figure 8).

Using high-temperature powder X-ray diffraction, the thermal expansion coefficient of La_3NbWO_{10} was calculated.

$$\beta = \frac{\Delta V}{V_o \times \Delta T}$$

$$\alpha = \beta/3 = 9.72 \times 10^{-6}(K^{-1})$$

The value is quite low in comparison to that of other materials (Table 6).

Table 6: Thermal expansion coefficients α of some materials in K^{-1}.

α-$La_2Mo_2O_9$	14.7×10^{-6}
β-$La_2Mo_2O_9$	18.1×10^{-6}
$La_{18}W_{10}O_{57}$	14.4×10^{-6}
La_2WO_6	11.6×10^{-6}
$La_{10}W_2O_{21}$	12.2×10^{-6}
$La_7Nb_3W_4O_{30}$	11.2×10^{-6}

The low ionic conductivity of La_3NbWO_{10} can be explained by the fact that the vacancies are not located in tunnels but in zigzag paths in which oxygen atoms can not move easily from one position to another, in addition to the low thermal expansion.

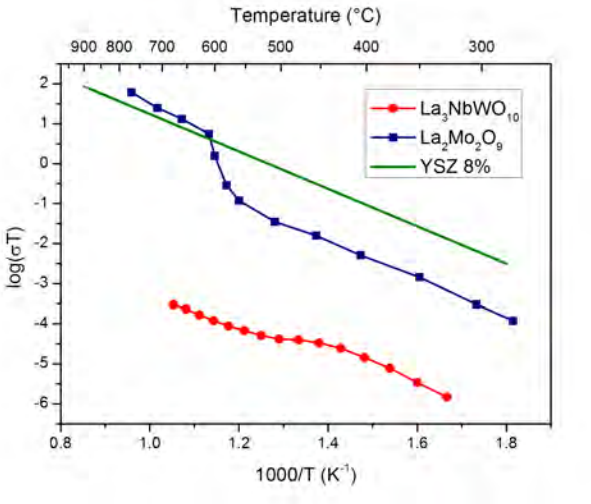

Figure 8: Arrhenius plot of the La_3NbWO_{10} compound, $La_2Mo_2O_9$ and YSZ 8%.

4. Conclusion

The investigation of the La_2O_3-WO_3-Nb_2O_5 phase diagram allowed us to discover the La_3NbWO_{10} phase, which constitutes the second ternary compound in this diagram. The structure of this new material, ab-initio determined from powder X-ray diffraction data, is a superstructure ($2a_F \times 2a_F \times 2a_F$) of the Fluorite family with a lengthened cell parameter a_F along the c axis. Two different formulations were used to describe the structure: i) $La_{18}Nb_6W_6\square_2O_{60}\square_4$ for the explanation of two cationic and four anionic vacancies and ii) ($[La_3] + 2 \times [(Nb/W)O_5]$) for the global view of layers and ribbons. The ionic conductivity of the compound is lower than that of $La_2Mo_2O_9$ and YSZ 8% because of the positions of its vacancies. Indeed, the low ion conductivity is attributed to the crystallographic distribution of vacancies that follow a zig-zag pathway, contrarily to zirconia that displays a tunnel arrangement of vacancies. This structure-property relationship confirms further our previous observations and helps to design specific materials with appropriate arrangement of vacancies in order to ameliorate the ionic conductivity properties.

[1] L. Malavasi, C. A. J. Fisher, M. S. Islam, Oxide-ion and proton conducting electrolyte materials for clean energy applications: structural and mechanistic features, Chemical Society Reviews 39 (11) (2010) 4370.
[2] B. C. H. Steele, Material science and engineering: The enabling technology for the commercialisation of fuel cell systems, Journal of Materials Science 36 (2001) 1053–1068.
[3] N. Minh, Solid oxide fuel cell technology-features and applications, Solid State Ionics 174 (1-4) (2004) 271–277.
[4] P. Lacorre, F. Goutenoire, O. Bohnke, Designing fast oxide-ion conductors based on $La_2Mo_2O_9$, Nature 404 (2000) 856–858.
[5] J.-S. Ha, E. Lee, S.-T. Hong, H.-I. Yoo, A new potential electrolyte $Ba_{11}W_4O_{23}$: Novel structure and electrical conductivity, Solid State Ionics 179 (21-26) (2008) 1066–1070.
[6] C. A. Lopez, J. C. Pedregosa, D. G. Lamas, J. A. Alonso, The strongly defective double perovskite $Sr_{11}Mo_4O_{23}$: crystal structure in relation to ionic conductivity, Journal of Applied Crystallography 47 (4) (2014) 1395–1401.
[7] A. Magraso, C. Frontera, D. Marrero-Lopez, P. Nunez, New crystal structure and characterization of lanthanum tungstate La_6WO_{12} prepared by freeze-drying synthesis, Dalton Transactions (46) (2009) 10273.
[8] M.-H. Chambrier, A. Le Bail, F. Giovannelli, A. Redjamia, P. Florian, D. Massiot, E. Suard, F. Goutenoire, $La_{10}W_2O_{21}$: An anion-deficient fluorite-related superstructure with oxide ion conduction, Inorganic Chemistry 53 (1) (2014) 147–159.
[9] I. R. Evans, J. A. Howard, J. S. Evans, The crystal structure of α-$La_2Mo_2O_9$ and the structural origin of the oxide ion migration pathway, Chemistry of materials 17 (16) (2005) 4074–4077.
[10] F. Dubois, F. Goutenoire, Y. Laligant, E. Suard, P. Lacorre, Ab-initio determination of $La_2Mo_4O_{15}$ crystal structure from X-rays and Neutron Powder Diffraction, Journal of Solid State Chemistry 159 (1) (2001) 228–233, pas de conduction ionique, structure pas jolie.
[11] V. Brizé, S. Georges, S. Kodjikian, E. Suard, F. Goutenoire, $La_6Mo_8O_{33}$: a new ordered defect scheelite superstructure, Journal of Solid State Chemistry 177 (7) (2004) 2617–2627.
[12] M. Yoshimura, High temperature phase relation in the system La_2O_3-WO_3, Materials Research Bulletin 11 (1976) 151–158.
[13] R. Roth, J. Waring, Phase equilibria as related to crystal structure in the system niobium pentoxide-tungsten trioxide, Journal of research of the National Bureau of Standards, 70A 4 (1966) 281–303.
[14] M.-H. Chambrier, R. Ibberson, F. Goutenoire, Structure determination of α-$La_6W_2O_{15}$, Journal of Solid State Chemistry 183 (6) (2010) 1297–1302. doi:10.1016/j.jssc.2010.03.043.
[15] M. Allix, M.-H. Chambrier, E. Véron, F. Porcher, M. Suchomel, F. Goutenoire, Synthesis and structure determination of the high temperature form of La_2WO_6, Crystal Growth & Design 11 (11) (2011) 5105–5112.
[16] M.-H. Chambrier, S. Kodjikian, R. Ibberson, F. Goutenoire, Ab-initio structure determination of β-La_2WO_6, Journal of Solid State Chemistry 182 (2) (2009) 209–214.
[17] M.-H. Chambrier, A. Le Bail, S. Kodjikian, E. Suard, F. Goutenoire, Structure determination of $La_{18}W_{10}O_{57}$, Inorganic Chemistry 48 (14) (2009) 6566–6572.
[18] Y. Laligant, A. Le Bail, F. Goutenoire, Ab Initio Structure Determination of Lanthanum Cyclo-tetratungstate α-$La_2W_2O_9$ from X-ray and Neutron Powder Diffraction, Journal of Solid State Chemistry 159 (1) (2001) 223–227.
[19] F. Goutenoire, S. Kodjikian, E. Suard, Extension of the $La_7Mo_7O_{30}$ structural type with $La_7Nb_3W_4O_{30}$ and $La_7Ta_3W_4O_{30}$ compounds, Journal of Solid State Chemistry 178 (9) (2005) 2811–2817.
[20] N. Almelo, X'Pert High Score Plus, PANalytical (2004).
[21] T. Timchenko, L. Petushkova, E. Pobedimskaya, A. Pashkova, A New Lanthanum Oxytungstate $2La_2O_3$- $3WO_3$, in: Soviet Physics Doklady, Vol. 14, 1969, p. 188.
[22] P. E. Werner, Trial-and-error computer methods for the indexing of unknown powder patterns, Zeitschrift fr Kristallographie 120 (1964) 375–387.
[23] J. Rodriguez-Carvajal, FullProfSuite Program.
[24] P. M. de Wolff, A simplified criterion for the reliability of a powder pattern indexing, Journal of Applied Crystallography 1 (2) (1968) 108–113.
[25] A. Le Bail, Monte carlo indexing with mcmaille, Powder

Diffraction 19 (03) (2004) 249–254.
[26] A. Le Bail, Espoir: A program for solving structures by Monte Carlo analysis of powder diffraction data, Materials Science Forum 378-381 (2001) 65–70.
[27] H. M. Rietveld, A profile refinement method for nuclear and magnetic structures, Journal of Applied Crystallography 2 (2) (1969) 65–71.
[28] P. Thompson, D. E. Cox, J. B. Hastings, Rietveld refinement of Debye-Scherrer synchrotron X-ray data from Al_2O_3, Journal of Applied Crystallography 20 (2) (1987) 79–83.
[29] D. Errandonea, J. Pellicer-Porres, F. Manjón, A. Segura, C. Ferrer-Roca, R. Kumar, O. Tschauner, P. Rodríguez-Hernández, J. López-Solano, S. Radescu, et al., High-pressure structural study of the scheelite tungstates $CaWO_4$ and $SrWO_4$, Physical Review B: Condensed Matter 72 (17) (2005) 174106.